Universidade de São Paulo
Biblioteca Digital da Produção Intelectual - BDPI

Departamento de Telecomunicações e Controle - EP/PTC
Artigos e Materiais de Revistas Científicas - EP/PTC

2012

Comparison of multiple-input single-output single-user ultra-wideband systems with pre-distortion

TRANSACTIONS ON EMERGING TELECOMMUNICATIONS TECHNOLOGIES, HOBOKEN, v. 23, n. 3, supl. 1, Part 3, pp. 240-253, APR, 2012
http://www.producao.usp.br/handle/BDPI/36821

Downloaded from: Biblioteca Digital da Produção Intelectual - BDPI, Universidade de São Paulo

TRANSACTIONS ON EMERGING TELECOMMUNICATIONS TECHNOLOGIES
Trans. Emerging Tel. Tech. 2012; **23**:240–253
Published online 5 Decemeber 2011 in Wiley Online Library (wileyonlinelibrary.com). DOI: 10.1002/ett.1528

RESEARCH ARTICLE

Comparison of multiple-input single-output single-user ultra-wideband systems with pre-distortion

B. A. Angélico[1], P. J. E. Jeszensky[2], P. M. S. Burt[2], W. S. Hodgkiss[3] and T. Abrão[4]*

[1] Federal Technology University of Paraná (UTFPR), Cornélio Procópio, Brazil
[2] Department of Telecommunications and Control Engineering, Escola Politécnica, University of São Paulo, São Paulo, Brazil
[3] Department of Electrical and Computer Engineering, University of California–San Diego, San Diego, CA, USA
[4] Department of Electrical Engineering, State University of Londrina, Londrina, Paraná, Brazil

ABSTRACT

This paper presents a performance analysis of a baseband multiple-input single-output ultra-wideband system over scenarios CM1 and CM3 of the IEEE 802.15.3a channel model, incorporating four different schemes of pre-distortion: time reversal, zero-forcing pre-equaliser, constrained least squares pre-equaliser, and minimum mean square error pre-equaliser. For the third case, a simple solution based on the steepest-descent (gradient) algorithm is adopted and compared with theoretical results. The channel estimations at the transmitter are assumed to be truncated and noisy. Results show that the constrained least squares algorithm has a good trade-off between intersymbol interference reduction and signal-to-noise ratio preservation, providing a performance comparable to the minimum mean square error method but with lower computational complexity. Copyright © 2011 John Wiley & Sons, Ltd.

***Correspondence**
T. Abrão, Department of Electrical Engineering, State University of Londrina, Rod. Celso Garcia Cid-PR445, s/n, Campus Universitário, 86051-970, PO Box 6001, Londrina, Paraná, Brazil.
E-mail: taufik@uel.br

Received 11 October 2010; Revised 20 September 2011; Accepted 22 September 2011

1. INTRODUCTION

Ultra-wideband (UWB) is an emerging technology that employs ultra-short pulses to transmit information, resulting in a very large bandwidth. Because of its attractive characteristics, such as very high data rates, low probability of interception and good time domain resolution allowing location and tracking applications at centimetre level, UWB has been considered as a promising solution for short-distance high-data-rate communications, such as wireless personal area networks.

Ultra-wideband channel is characterised by a dense multipath environment. For the energy spread over the multipath components to be effectively captured, the transmit-based time reversal (TR) technique (sometimes called pre-Rake) has been investigated [1–6]. In baseband TR, the channel impulse response (CIR) is estimated from a probe signal, and the data are convolved with the complex conjugate time-reversed version of the estimated CIR (namely, TR coefficients) prior to transmission. This technique is based on the channel reciprocity, which was experimentally verified in [1] for a particular UWB environment. TR-based UWB transmission can provide intersymbol interference (ISI) mitigation by reducing the delay spread of the channel and also co-channel interference rejection by focusing the signal on the point of interest.

However, for high transmission rates, the residual ISI will still degrade the system performance because the equivalent CIR after TR* is not a delta function. In order to handle such impairments, we can employ a receiver-based channel equalisation scheme with fewer taps than that used without TR [7–9].

In wireless communications, it is sometimes desired to keep portable devices as simple and as power efficient as possible. From this standpoint, a receiver-based equaliser may aggregate an undesired complexity to the

*The term equivalent CIR refers to the convolution between the TR coefficients and the original CIR. In a multiple-input single-output (MISO) system, it is the summation of the resultant convolutions from each transmit antenna element.

Copyright © 2011 John Wiley & Sons, Ltd.

receiver in a downlink scenario. Hence, some transmitter-based equalisation can be applied to mitigate ISI, without adding complexity to the receiver. In [10], the authors compared the performance of pure TR with a zero-forcing (ZF) pre-equalised system, for fixed wireless access channels, and also proposed a new joint ZF and TR scheme. In [11], the authors proposed additional spatial and frequency filters to the ZF and TR pre-filters over an IEEE 802.11n channel model. In [12], two novel minimum mean square error (MMSE)-based symbol-level pre-equalisation for MISO direct-sequence UWB (DS-UWB) systems in cascade with pre-Rake combining are proposed and shown to achieve a good bit error rate (BER) performance.

In this work, a performance comparison of a downlink MISO UWB system with four different schemes of pre-distortion is presented. An objective function modeled as a constrained least squares (CLS) problem is considered. Imperfect channel estimation, no coding and perfect data synchronisation are considered. The transmission is assumed to be from an access point with relatively good computational capacity to a lower complexity device with hardware constraints. When the number of transmit antennas is $N_t > 1$, it is assumed that the small-scale fading components across antennas are independent, but the shadowing factors are correlated, according to the method in [13].

Overall, despite many papers in the field of impulse UWB considering a carrier-free pulse, the IEEE 802.15.3a DS-UWB [14] standard, as well as the IEEE 802.15.4a UWB standard [15], assumes a square-root raised-cosine (RRC) pulse that requires a carrier. All the schemes presented in this paper are performed in baseband considering an RRC pulse shape.

The rest of the paper has the following organisation. Section 2 describes the UWB channel and system model. Section 3 considers the derivation of pre-filter coefficients, whereas Section 4 presents a complexity analysis, and Section 5 considers the signal-to-interference-plus-noise rate (SINR) analysis. Section 6 shows the simulation parameters and results, whereas Section 7 points out the main conclusions.

2. CHANNEL AND SYSTEM MODEL

2.1. Channel model

A discrete-time complex baseband version of the IEEE 802.15.3a model is used [16, 17], where multipath components arrive in clusters. Cluster and ray arrivals within each cluster are Poisson distributed with rate Λ and $\lambda > \Lambda$, respectively. The arrival times of the ℓ_1th cluster and the ℓ_2th ray within the ℓ_1th cluster are denoted by τ_{ℓ_1} and τ_{ℓ_1,ℓ_2}. The multipath gain β_{ℓ_1,ℓ_2} is described by a log-normal distribution, and its phase assumes only 0 or π with equal probability. A channel realisation at kth antenna

Table I. Channel parameters for CM1 and CM3 of IEEE 802.15.3a model.

Parameters	CM1	CM3
Λ (1/ns)	0.0233	0.0667
λ (1/ns)	2.5	2.1
σ_1 (dB)	3.39	3.39
σ_2 (dB)	3.39	3.39
σ_x (dB)	3	3

consists of

$$h_k^{'}(t) = \chi_k \sum_{\ell_1=0}^{L_1-1} \sum_{\ell_2=0}^{L_2-1} \beta_{\ell_1,\ell_2}^k \, \delta\left(t - \tau_{\ell_1}^k - \tau_{\ell_1,\ell_2}^k\right) \quad (1)$$

where $\delta(\cdot)$ is the Dirac delta function and $\chi_k = 10^{(\sigma_\chi/20)\, w_k}$ is the log-normal shadowing associated with the Gaussian random variable (r.v.) w_k, with $\sigma_\chi = 3$ dB being the standard deviation of χ_k [16]. Two scenarios are considered: CM1 and CM3. Table I summarises the channel parameters [16].

The terms σ_1 and σ_2 are respectively the standard deviation of cluster log-normal fading (β_{ℓ_1,ℓ_2}^k for a fixed ℓ_2) and ray log-normal fading (β_{ℓ_1,ℓ_2}^k for a fixed ℓ_1).

The kth discrete-time complex baseband CIR with sampling interval T and length L is obtained by [12]

$$h_k[m] = g_T(t) * h_k^{''}(t) * g_R(t)\Big|_{mT} \quad (2)$$

where T is the reciprocal of the symbol rate, $*$ denotes convolution, $g_R(t)$ is matched to the pulse $g_T(t)$, which has an RRC shape, and $h_k^{''}(t)$ is a baseband version of $h_k^{'}(t)$. Here, parameter T is used for the pulse generation, but the effective symbol rate is controlled by the interval between consecutive symbols, $T_s = \kappa T$, where κ is an integer.[†] According to [13], the multipath components are independent across antennas, but the shadowing terms χ_k are correlated. Therefore, the CIRs are normalised before inserting the shadowing effect, which for the three antenna cases has the following correlation matrix [13]

$$\mathbf{R}_\chi = \begin{bmatrix} 1 & 0.86 & 0.54 \\ 0.86 & 1 & 0.86 \\ 0.54 & 0.86 & 1 \end{bmatrix} \quad (3)$$

For two transmitter antennas, $\mathbf{R}_\chi$ is a 2×2 matrix with 0.86 in the secondary diagonal. Considering ρ_{χ_k,χ_j}, the correlation coefficient between the log-normal variables χ_k, χ_j, and ρ_{w_k,w_j}, the correlation coefficient between

[†]In fact, if there was no time interval (multiple of T) between consecutive symbols, $1/T$ would be the effective symbol rate.

the Gaussian variables w_k , w_j, related to χ_k, χ_j, it was shown in [13] that

$$\rho_{w_k,w_j} = \frac{1}{\xi^2\sigma_\chi^2} \ln\left\{\left(e^{\xi^2\sigma_{\chi^2}} - 1\right)\rho_{\chi_k,\chi_j} + 1\right\} \quad (4)$$

with $\xi = \ln(10)/2$.

Hence, from ρ_{w_k,w_j}, a Gaussian correlated vector of size N_t is obtained. Finally, a log-normal correlated vector of size N_t is obtained according to $\chi_k = 10(\sigma_\chi/20)w_k$.

The discrete-time CIR with resolution T, length L and correlated shadowing is given by

$$h_k[m] = \sum_{\ell=0}^{L-1} \alpha_\ell^k \delta[m-\ell] \quad (5)$$

2.2. Channel estimation

Because of the large number of resolvable paths, the CIR on each antenna is truncated to obtain the TR coefficients. The criterion for this truncation is illustrated in Figure 1. The normalised power delay profile does not take into account the interval (zero samples) before the first significant path. Mainly in the scenario CM3, there might exist a relative delay between the first significant path on each antenna element. However, such a delay must be reinserted in the estimated channels in order to properly combine the components from each antenna. As the original channel model does not consider multiple antennas, the maximum relative delay among CIRs was fixed at 2.505 ns, which corresponds to five times the channel resolution.

Moreover, the TR coefficients are obtained, considering estimate errors. The method for generating CIR estimation errors is based on [4]. Assuming a time duplex division system, a sequence of N_P probe pulses with a repetition period longer than the maximum effective delay spread of the channel, τ_{ef}, is transmitted from the receiver to the transmitter side. Assuming perfect synchronisation, the N_P CIR realisations estimated on each antenna are coherently averaged. If the additive white Gaussian noise (AWGN) double-sided power spectral density per antenna is given by $N_0/2$, the signal-to-noise ratio (SNR) per antenna is defined as

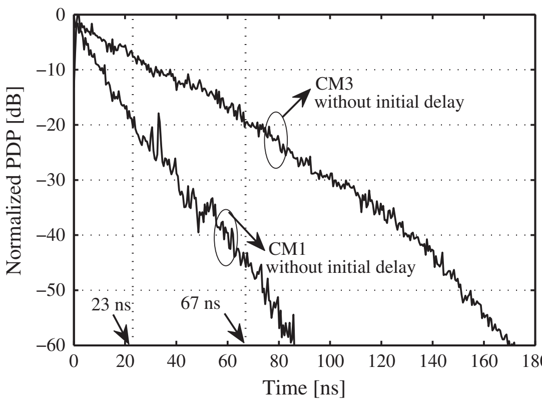

Figure 1. Normalised power delay profile (PDP) for CM1 and CM3, not considering the zero samples before the first significant path. A −20-dB criterion is chosen for the CIR truncation on each antenna.

$$SNR = \frac{E_b^k}{N_0} \quad (6)$$

where $E_b^k = E_b/N_t$ is the mean bit energy per antenna, considering N_t antennas. Assuming a static channel during the frame period, the estimated coefficients on the kth antenna, $\left\{\tilde{\alpha}_\ell^k\right\}_{\ell=0}^{L-1}$, are represented as

$$\tilde{\alpha}_\ell^k = \frac{1}{N_P}\sum_{n=1}^{N_P} \tilde{\alpha}_\ell^k(n) = \alpha_\ell^k + e_\ell^k, \quad (7)$$

with e_ℓ^k being a complex Gaussian r.v. that represents the noise of the imperfect channel estimation on the ℓth resolvable path, with variance of the in-phase and quadrature components given by $N_0/2\,N_P$ [4]. The estimated discrete-time CIR after truncation is defined as $\tilde{h}_k[m]$, with length L_C. It is important to note that channel estimation errors are not explicitly shown in the results. However, in all cases, the pre-filter coefficients are obtained, taking into account the estimated CIR, which is noisy and truncated.

2.3. System model

The discrete-time model considered is shown in Figure 2. γ_k represents the sequence of pre-filter coefficients on the kth antenna, and $z[m]$ is the sampled AWGN. Signals and systems are represented by their complex baseband equivalents. For antipodal binary signalling with symbols $b_i \in \{\pm 1\}$ and N_t antennas, the signal to be transmitted on the kth antenna element is represented as

$$s_k[m] = \sqrt{E_b^k}\sum_{i=-\infty}^{\infty} b_i\,\gamma_k[m - i\kappa] \quad (8)$$

with $\gamma_k[m]$ representing the pre-filter on the kth antenna. Considering perfect synchronisation, the output of the receive matched filter (MF), resampled at the rate $1/T_s$, is

$$y[n] = \sum_{i=-\infty}^{\infty} b_i\,x[n-i] + z[n] \quad (9)$$

where $z[n]$ is the discrete-time AWGN at the output of the MF and $x[n]$ denotes the equivalent CIR, which is obtained from

$$x[m] = \sqrt{E_b^k}\sum_{k=1}^{N_t}(\gamma_k * h_k)[m] \quad (10)$$

Trans. Emerging Tel. Tech. **23**:240–253 (2012) © 2011 John Wiley & Sons, Ltd.
DOI: 10.1002/ett

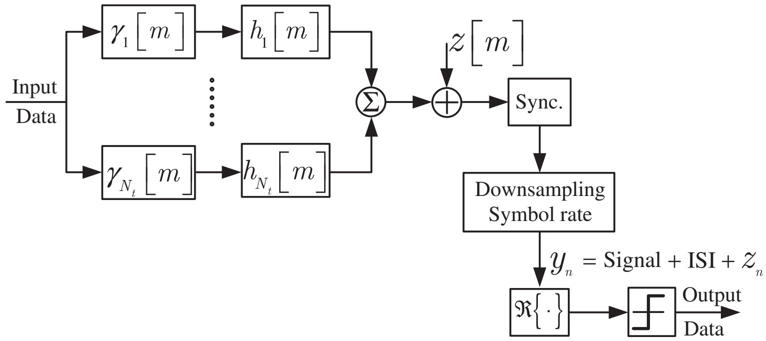

Figure 2. Equivalent discrete-time model. ISI represents the intersymbol interference, $y_n = y(nT_s)$ and $z_n = z(nT_s)$.

downsampling it by a factor of $\kappa = T_s/T$. Assuming $E_b^k = 1$, the variance of the AWGN per antenna, $z_k[m]$, $k = 1, \cdots, N_t$, is given by $\sigma_k^2 = 1/SNR$ (the same for each antenna).

3. PRE-FILTER COEFFICIENTS

In all the schemes considered, the length of the pre-filter on each antenna is set as $L_{\text{PF}} \leqslant L_{\text{C}}$. An estimate of $x[m]$ from Equation (10) in a matrix-vector notation can be obtained as

$$\tilde{\mathbf{x}} = \tilde{\mathbf{H}}\boldsymbol{\gamma} \tag{11}$$

where $\boldsymbol{\gamma} = \left[\left(\boldsymbol{\gamma}^0\right)^\top \cdots \left(\boldsymbol{\gamma}^{L_{\text{PF}}-1}\right)^\top\right]^\top$ is a $(N_t\, L_{\text{PF}}) \times 1$ vector with $\boldsymbol{\gamma}^\ell = \left[\gamma_1[\ell] \cdots \gamma_{N_t}[\ell]\right]^\top$, with $\{\cdot\}^\top$ meaning transposition; $\tilde{\mathbf{H}}$ is a $p \times q$ block Toeplitz matrix, where $p = L_{\text{C}} + L_{\text{PF}} - 1$ and $q = N_t L_{\text{PF}}$, given by

$$\tilde{\mathbf{H}} = \begin{bmatrix} \left(\tilde{\mathbf{h}}^0\right)^\top & \mathbf{0}^\top & \cdots & \mathbf{0}^\top \\ \left(\tilde{\mathbf{h}}^1\right)^\top & \left(\tilde{\mathbf{h}}^0\right)^\top & \ddots & \vdots \\ \vdots & \left(\tilde{\mathbf{h}}^1\right)^\top & \ddots & \mathbf{0}^\top \\ \left(\tilde{\mathbf{h}}^{L_{\text{C}}-1}\right)^\top & \vdots & \ddots & \left(\tilde{\mathbf{h}}^0\right)^\top \\ \mathbf{0}^\top & \left(\tilde{\mathbf{h}}^{L_{\text{C}}-1}\right)^\top & & \left(\tilde{\mathbf{h}}^1\right)^\top \\ \vdots & \ddots & \ddots & \vdots \\ \mathbf{0}^\top & \cdots & \mathbf{0}^\top & \left(\tilde{\mathbf{h}}^{L_{\text{C}}-1}\right)^\top \end{bmatrix} \tag{12}$$

whose first N_t columns are padded with $L_{\text{PF}} - 1$ null vectors, $\mathbf{0}^\top$, with length N_t and $\tilde{\mathbf{h}}^\ell = \left[\tilde{h}_1[\ell] \cdots \tilde{h}_{N_t}[\ell]\right]^\top$. After obtaining $\boldsymbol{\gamma}$, we reshaped it into a matrix of N_t rows and L_{PF} columns, whose kth row represents the pre-filter coefficients on the kth antenna element, $\boldsymbol{\gamma}_k = [\gamma_k[0], \cdots, \gamma_k[L_{\text{PF}} - 1]]$.

3.1. Time reversal pre-filter

Time reversal coefficients on the kth antenna, $\boldsymbol{\gamma}_k = \boldsymbol{\gamma}_k^{\text{TR}} = \left[\gamma_k^{\text{TR}}[0] \cdots \gamma_k^{\text{TR}}[L_{\text{PF}} - 1]\right]$, are obtained as

$$\gamma_k^{\text{TR}}[m] = C_k \left(\tilde{h}_k[-m]\right)^* \tag{13}$$

where the constant C_k depends on the power allocation scheme.‡ In this paper, C_k is set to be equal for all the antenna elements, that is,

$$C_k = C = \sqrt{\frac{N_t}{\sum_{k=1}^{N_t} \left\|\tilde{\mathbf{h}}_k\right\|_2^2}} \tag{14}$$

with $\tilde{\mathbf{h}}_k = \left[\tilde{h}_k[0] \cdots \tilde{h}_k[L_{\text{PF}} - 1]\right]$ being the vector of estimated taps for each antenna element. Note that the total energy of the normalised coefficients from all N_t antennas is equal to N_t. It is possible to see that the vector of TR coefficients for all N_t antennas, $\boldsymbol{\gamma} = \boldsymbol{\gamma}^{\text{TR}}$, is given by the (L_{PF})th line of the matrix $\tilde{\mathbf{H}}$ in Equation (12), multiplied by the normalisation factor C_k.

3.2. Zero-forcing pre-equaliser

The ZF pre-equaliser attempts to cancel the ISI. Here, the ZF coefficients for all N_t antennas, $\boldsymbol{\gamma} = \boldsymbol{\gamma}^{\text{ZF}}$, are obtained, considering that

$$\tilde{\mathbf{H}}\boldsymbol{\gamma}^{\text{ZF}} = \psi\, \mathbf{d}_v \tag{15}$$

where $\mathbf{d}_v = [0, \cdots, 0, 1, 0, \cdots, 0]^\top$ has length p, with 1 at the vth position. v and ψ are specified below. The ZF solution is given by

$$\boldsymbol{\gamma} = \boldsymbol{\gamma}^{\text{ZF}} = \psi\, \tilde{\mathbf{H}}^\dagger\, \mathbf{d}_v \tag{16}$$

‡For a causal representation, $h_k^{\text{TR}}[m] = C_k \left(\tilde{h}_k[L_{\text{PF}} - m - 1]\right)^*$ should have been assumed, but it does not change the theoretical results because we are further considering that the index **0**th represents the information timing.

with $\tilde{\mathbf{H}}^{\dagger}$ being the pseudo-inverse of $\tilde{\mathbf{H}}$. If $q > p$ and rank $(\tilde{\mathbf{H}}) = p$, there are many solutions. One particular solution is $\tilde{\mathbf{H}}^{\dagger} = \tilde{\mathbf{H}}^{H}\left(\tilde{\mathbf{H}}\tilde{\mathbf{H}}^{H}\right)^{-1}$, which minimises $\left\|\tilde{\mathbf{H}}\boldsymbol{\gamma}^{\mathrm{ZF}} - \psi\mathbf{d}_{v}\right\|_{2}^{2}$. In this case, v is selected in order to maximise ψ because it determines the power of the received signal [10]. Assuming $\|\boldsymbol{\gamma}^{\mathrm{ZF}}\|_2^2 = N_t$, it follows that

$$
\begin{aligned}
&\left\|\boldsymbol{\gamma}^{\mathrm{ZF}}\right\|^{2} = N_t\\
&\Rightarrow |\psi|^{2}\,\mathbf{d}_{v}\left(\tilde{\mathbf{H}}\tilde{\mathbf{H}}^{H}\right)^{-1}\tilde{\mathbf{H}}\tilde{\mathbf{H}}^{H}\left(\tilde{\mathbf{H}}\tilde{\mathbf{H}}^{H}\right)^{-1}\mathbf{d}_{v} = N_t\\
&\Rightarrow |\psi|^{2}\left[\left(\tilde{\mathbf{H}}\tilde{\mathbf{H}}^{H}\right)^{-1}\right]_{v,v} = N_t
\end{aligned}
\tag{17}
$$

Hence, v is chosen so that $\left[\left(\tilde{\mathbf{H}}\tilde{\mathbf{H}}^{H}\right)^{-1}\right]_{v,v}$ is minimum. Note that the condition $N_t \geqslant 2$ must be satisfied for a ZF solution. If $N_t = 2$, L_{PF} cannot be smaller than L_{C}.

On the other hand, if $p > q$ and rank $(\tilde{\mathbf{H}}) = q$, a ZF solution cannot be guaranteed. However, v can be fixed as $v = L_{\mathrm{PF}}$, for example, and an approximated solution (denoted by ZF′) that minimises $\left\|\tilde{\mathbf{H}}\boldsymbol{\gamma} - \mathbf{d}_{v}\right\|_{2}^{2}$ can be obtained as $\boldsymbol{\gamma} = \tilde{\mathbf{H}}^{\dagger}\mathbf{d}_{v}$, where $\tilde{\mathbf{H}}^{\dagger} = \left(\tilde{\mathbf{H}}^{H}\tilde{\mathbf{H}}\right)^{-1}\tilde{\mathbf{H}}^{H}$. This solution has to be normalised in order to generate a power-constrained solution given by $\boldsymbol{\gamma}^{\mathrm{ZF}'} = \sqrt{N_t/\|\boldsymbol{\gamma}\|_2^2}\,\boldsymbol{\gamma}$.

3.3. Constrained least squares pre-equaliser

Because $\tilde{\mathbf{h}}_k$ is available at the transmitter, let $\underline{\tilde{\mathbf{h}}}_k = C\,\tilde{\mathbf{h}}_k$ be a normalised version of $\tilde{\mathbf{h}}_k$. Thus, a normalised estimation of $x[m]$ in a matrix-vector can be obtained as

$$
\underline{\tilde{\mathbf{x}}} = \underline{\tilde{\mathbf{H}}}\boldsymbol{\gamma}
\tag{18}
$$

where $\underline{\tilde{\mathbf{H}}}$ is given by Equation (12), substituting $\underline{\tilde{\mathbf{h}}}^{\ell} = C_k\left[\tilde{h}_1[\ell]\cdots\tilde{h}_{N_t}[\ell]\right]^{\top}$ for $\tilde{\mathbf{h}}^{\ell} = \left[\tilde{h}_1[\ell]\cdots\tilde{h}_{N_t}[\ell]\right]^{\top}$.

Considering a power constraint $\|\boldsymbol{\gamma}\|_2^2 \leqslant N_t$, the idea of the CLS equaliser is to make $\underline{\tilde{\mathbf{x}}}$ be as close as possible to the vector $\mathbf{d} = [0\cdots N_t\cdots 0]^{\top}$ with length p and N_t at position L_{PF}. Defining $J_{\mathrm{CLS}} = \|\underline{\tilde{\mathbf{x}}} - \mathbf{d}\|_2^2$, we can obtain $\boldsymbol{\gamma} = \boldsymbol{\gamma}^{\mathrm{CLS}}$ as

$$
\begin{aligned}
&\min_{\boldsymbol{\gamma}} J_{\mathrm{CLS}}\\
&\text{s.t. } \|\boldsymbol{\gamma}\|_2^2 \leqslant N_t
\end{aligned}
\tag{19}
$$

In [18], a solution for the CLS problem using the singular-value decomposition (SVD) of $\underline{\tilde{\mathbf{H}}}$ and Lagrange multipliers is presented and named least squares minimisation over a sphere. The matrix $\underline{\tilde{\mathbf{H}}}$ is decomposed, such that $\mathbf{U}^{H}\underline{\tilde{\mathbf{H}}}\mathbf{V} = \boldsymbol{\Sigma}_{\underline{\tilde{\mathbf{H}}}}$, where $\mathbf{V} = \left[\mathbf{v}_1\ \mathbf{v}_2\ \cdots\ \mathbf{v}_q\right]$ $(q\times q)$ and $\mathbf{U} = \left[\mathbf{u}_1\ \mathbf{u}_2\ \cdots\ \mathbf{u}_p\right]$ $(p\times p)$ are unitary matrices, whereas $\boldsymbol{\Sigma}_{\underline{\tilde{\mathbf{H}}}}$ is the matrix (not necessarily square) whose diagonal elements are the singular values of $\underline{\tilde{\mathbf{H}}}$. With this transformation,

$$
\begin{aligned}
\left\|\mathbf{U}^{H}\left(\underline{\tilde{\mathbf{H}}}\boldsymbol{\gamma} - \mathbf{d}\right)\right\|_2^2 &= \left\|\mathbf{U}^{H}\left(\underline{\tilde{\mathbf{H}}}\mathbf{V}\mathbf{V}^{H}\boldsymbol{\gamma} - \mathbf{d}\right)\right\|_2^2\\
&= \left\|\mathbf{U}^{H}\underline{\tilde{\mathbf{H}}}\mathbf{V}\mathbf{V}^{H}\boldsymbol{\gamma} - \mathbf{U}^{H}\mathbf{d}\right\|_2^2\\
&= \left\|\boldsymbol{\Sigma}_{\underline{\tilde{\mathbf{H}}}}\tilde{\boldsymbol{\gamma}} - \tilde{\mathbf{d}}\right\|_2^2
\end{aligned}
\tag{20}
$$

where $\tilde{\mathbf{d}} = \mathbf{U}^{H}\mathbf{d}$, $\tilde{\boldsymbol{\gamma}} = \mathbf{V}^{H}\boldsymbol{\gamma}$ and $\{\cdot\}^{H}$ the Hermitian operator. Note that $\|\tilde{\boldsymbol{\gamma}}\|_2^2 = \left\|\mathbf{V}^{H}\boldsymbol{\gamma}\right\|_2^2 = \|\boldsymbol{\gamma}\|_2^2$. Therefore, the following Lagrange problem is obtained

$$
\mathcal{L}(\tilde{\boldsymbol{\gamma}},\lambda) = \left(\boldsymbol{\Sigma}_{\underline{\tilde{\mathbf{H}}}}\tilde{\boldsymbol{\gamma}} - \tilde{\mathbf{d}}\right)^{H}\left(\boldsymbol{\Sigma}_{\underline{\tilde{\mathbf{H}}}}\tilde{\boldsymbol{\gamma}} - \tilde{\mathbf{d}}\right) + \lambda\left(\tilde{\boldsymbol{\gamma}}^{H}\tilde{\boldsymbol{\gamma}} - N_t\right)
\tag{21}
$$

with λ being the Lagrange multiplier. With $\mathcal{L}(\tilde{\boldsymbol{\gamma}},\lambda)$ being differentiated with respect to $\tilde{\boldsymbol{\gamma}}^{*}$ and the resulting gradient being set to zero, it follows that

$$
\begin{aligned}
\frac{\partial\mathcal{L}(\tilde{\boldsymbol{\gamma}},\lambda)}{\partial\tilde{\boldsymbol{\gamma}}^{*}} = 0 &\Rightarrow \boldsymbol{\Sigma}_{\underline{\tilde{\mathbf{H}}}}^{\top}\left(\boldsymbol{\Sigma}_{\underline{\tilde{\mathbf{H}}}}\tilde{\boldsymbol{\gamma}} - \tilde{\mathbf{d}}\right) + \lambda\tilde{\boldsymbol{\gamma}} = 0\\
&\Rightarrow \left(\lambda I + \boldsymbol{\Sigma}_{\underline{\tilde{\mathbf{H}}}}^{\top}\boldsymbol{\Sigma}_{\underline{\tilde{\mathbf{H}}}}\right)\tilde{\boldsymbol{\gamma}} = \boldsymbol{\Sigma}_{\underline{\tilde{\mathbf{H}}}}^{\top}\tilde{\mathbf{d}}
\end{aligned}
\tag{22}
$$

Hence, the CLS filter coefficients are given by

$$
\tilde{\boldsymbol{\gamma}} = \left[\frac{\sigma_1}{\lambda+\sigma_1^2}\tilde{d}_1\ \ \frac{\sigma_2}{\lambda+\sigma_2^2}\tilde{d}_2\ \ \cdots\ \ \frac{\sigma_r}{\lambda+\sigma_r^2}\tilde{d}_r\right]^{\top}
\tag{23}
$$

with the following constraint

$$
\sum_{i=1}^{r}\left(\frac{\sigma_i}{\lambda+\sigma_i^2}\right)^2\left|\tilde{d}_i\right|^2 = N_t
\tag{24}
$$

where r is the rank of the matrix $\underline{\tilde{\mathbf{H}}}$. Consequently, if $\sum_{i=1}^{r}\left|\tilde{d}_i\right|^2/\sigma_i^2 > N_t$, then

$$
\begin{aligned}
&\boldsymbol{\gamma} = \boldsymbol{\gamma}^{\mathrm{CLS}} = \sum_{i=1}^{r}\left(\frac{\sigma_i\tilde{d}_i}{\lambda^{*}+\sigma_i^2}\right)\mathbf{v}_i\\
&\lambda^{*} \leftarrow \sum_{i=1}^{r}\left(\frac{\sigma_i}{\lambda^{*}+\sigma_i^2}\right)^2\left|\tilde{d}_i\right|^2 = N_t
\end{aligned}
\tag{25}
$$

else,

$$
\boldsymbol{\gamma} = \boldsymbol{\gamma}^{\mathrm{CLS}} = \sum_{i=1}^{r}\left(\frac{\tilde{d}_i}{\sigma_i}\right)\mathbf{v}_i
\tag{26}
$$

The term λ^{*} can be found using, for instance, the bisection method. In order to find an iterative solution for the CLS problem, we firstly considered the unconstrained

Trans. Emerging Tel. Tech. **23**:240–253 (2012) © 2011 John Wiley & Sons, Ltd.
DOI: 10.1002/ett

problem. The gradient of J is $\nabla J = -2\underline{\tilde{\mathbf{H}}}^H\mathbf{e}$, where $\mathbf{e} = (\mathbf{d} - \underline{\tilde{\mathbf{H}}}\boldsymbol{\gamma}^{\mathrm{CLS}})$ is the error vector. In the steepest-descent algorithm, the coefficients on the $(i+1)$th iteration are updated as $\boldsymbol{\gamma}^{\mathrm{CLS}}(i+1) = \boldsymbol{\gamma}^{\mathrm{CLS}}(i) + \mu\left(\underline{\tilde{\mathbf{H}}}^H\mathbf{e}(i)\right)$, where μ is the convergence factor. This algorithm comes out with a solution that is unconstrained. Therefore, Algorithm 3.3 is proposed to generate an energy-constrained vector $\boldsymbol{\gamma}^{\mathrm{CLS}}$.

Algorithm 1 Modified Steepest Descent

Initialisation:

$\boldsymbol{\gamma}^{\mathrm{CLS}}(0) = \boldsymbol{\gamma}^{\mathrm{TR}} = \left[\left(\boldsymbol{\gamma}_0^{\mathrm{TR}}\right)^\top \cdots \left(\boldsymbol{\gamma}_{L_{\mathrm{PF}}-1}^{\mathrm{TR}}\right)^\top\right]^\top$;

$\boldsymbol{\gamma}_\ell^{\mathrm{TR}} = \left[\gamma_{\ell,1}^{\mathrm{TR}} \cdots \gamma_{\ell,N_t}^{\mathrm{TR}}\right]^\top$

for $i = 1, 2, \cdots$, ITER (Number of iterations)

$\mathbf{e}(i-1) = \mathbf{d} - \underline{\tilde{\mathbf{H}}}\boldsymbol{\gamma}^{\mathrm{CLS}}(i-1)$; (Error)

$\boldsymbol{\gamma}_{\mathrm{tmp}}^{\mathrm{CLS}} = \boldsymbol{\gamma}^{\mathrm{CLS}}(i-1) + \mu\underline{\tilde{\mathbf{H}}}^H\mathbf{e}(i-1)$ (Temp. coeff. update)

$\boldsymbol{\gamma}^{\mathrm{CLS}}(i) = \sqrt{\frac{N_t}{\left\|\boldsymbol{\gamma}_{\mathrm{tmp}}^{\mathrm{CLS}}\right\|_2^2}}\,\boldsymbol{\gamma}_{\mathrm{tmp}}^{\mathrm{CLS}}$ (Normalisation)

end

The coefficients are normalised right after the updating process within each iteration, and the error and gradient computations are performed with respect to those normalised coefficients. Figure 3 presents the convergence of the proposed CLS algorithm. The convergence factor μ is chosen as in the unconstrained gradient algorithm, that is, $0 < \mu < 2/\lambda_{\max}^{\mathbf{R}}$, where $\lambda_{\max}^{\mathbf{R}}$ represents the maximum eigenvalue of the matrix $\mathbf{R} = \underline{\tilde{\mathbf{H}}}^H\underline{\tilde{\mathbf{H}}}$. Note that 15 to 30 iterations are enough for achieving convergence.

3.4. Minimum mean square error pre-equaliser

Another possible power-constrained pre-equalisation is based on [12], where the filter coefficients are obtained by considering the MMSE criterion applied previously to a TR filter. In this paper, the MMSE filter will not be used in cascade with a TR filter but directly, like in the CLS scheme. Considering $\mathbf{b} = \left[b_{n+L_{\mathrm{PF}}-1} \cdots b_n \cdots b_{n-L_{\mathrm{C}}+1}\right]$, a vector of information bits with $L_{\mathrm{C}} + L_{\mathrm{PF}} - 1$ components and b_n at the (L_{PF})th position, the estimated received signal after MF can be written as

$$\tilde{y}_n = \mathbf{b}^H\tilde{\mathbf{x}} + z_n = \mathbf{b}^H\tilde{\mathbf{H}}\boldsymbol{\gamma} + z_n \tag{27}$$

Equation (27) is a non-causal representation, but this does not change the results. As considered in [12], the received signal is multiplied by a constant ζ in order to help the minimisation procedure. The design goal of the MMSE criterion is to minimise $J_{\mathrm{MMSE}} = \mathbb{E}\left[|b_n - \zeta\tilde{y}_n|^2\right]$, subjected to $\|\boldsymbol{\gamma}\|_2^2 = N_t$. J_{MMSE} is given by

$$\begin{aligned} J_{\mathrm{MMSE}} &= \mathbb{E}\left[|b_n - \zeta\tilde{y}_n|^2\right] = \mathbb{E}\left[(b_n - \zeta\tilde{y}_n)^*(b_n - \zeta\tilde{y}_n)\right] \\ &= \mathbb{E}\left[1 - b_n\zeta\tilde{y}_n - \zeta^*\tilde{y}_n^*b_n + |\zeta|^2|\tilde{y}_n|^2\right] \\ &= \mathbb{E}\left[1 - b_n\zeta(\mathbf{b}^H\underline{\tilde{\mathbf{H}}}\boldsymbol{\gamma} + z_n)\right. \\ &\qquad \left. -\zeta^*(\boldsymbol{\gamma}^H\tilde{\mathbf{H}}^H\mathbf{b} + z_n^*)b_n + |\zeta|^2|\tilde{y}_n|^2\right] \end{aligned} \tag{28}$$

The term $\mathbb{E}\left[|\tilde{y}_n|^2\right]$ in Equation (28) is given by

$$\begin{aligned} \mathbb{E}[|\tilde{y}_n|^2] &= \mathbb{E}\left[\left(\boldsymbol{\gamma}^H\tilde{\mathbf{H}}^H\mathbf{b} + z_n^*\right)\left(\mathbf{b}^\top\tilde{\mathbf{H}}\boldsymbol{\gamma} + z_n\right)\right] \\ &= \boldsymbol{\gamma}^H\tilde{\mathbf{H}}^H\tilde{\mathbf{H}}\boldsymbol{\gamma} + \sigma_z^2 \end{aligned} \tag{29}$$

Hence,

$$\begin{aligned} J_{\mathrm{MMSE}} &= 1 + |\zeta|^2\sigma_z^2 - \zeta^*\boldsymbol{\gamma}^H\mathbf{h}_n - \zeta\mathbf{h}_n^H\boldsymbol{\gamma} \\ &\quad + |\zeta|^2\boldsymbol{\gamma}^H\tilde{\mathbf{H}}^H\tilde{\mathbf{H}}\boldsymbol{\gamma} \end{aligned} \tag{30}$$

where $\mathbf{h}_n = \tilde{\mathbf{H}}^H\mathbb{E}[b_n\mathbf{b}] = \tilde{\mathbf{H}}^H\mathbf{d}_n$ and $\mathbf{d}_n$ is the vector whose elements are zero, except for the (L_{PF})th element, which is equal to 1. Defining $\bar{\boldsymbol{\gamma}} = \zeta\boldsymbol{\gamma}$ and noting that $|\zeta|^2 = (1/N_t)\bar{\boldsymbol{\gamma}}^H\bar{\boldsymbol{\gamma}}$, we automatically insert the power constraint in J_{MMSE} [12], resulting in

$$J_{\mathrm{MMSE}} = 1 + \frac{\sigma_z^2}{N_t}\bar{\boldsymbol{\gamma}}^H\bar{\boldsymbol{\gamma}} - \bar{\boldsymbol{\gamma}}^H\mathbf{h}_n - \mathbf{h}_n^H\bar{\boldsymbol{\gamma}} + \bar{\boldsymbol{\gamma}}^H\tilde{\mathbf{H}}^H\tilde{\mathbf{H}}\bar{\boldsymbol{\gamma}} \tag{31}$$

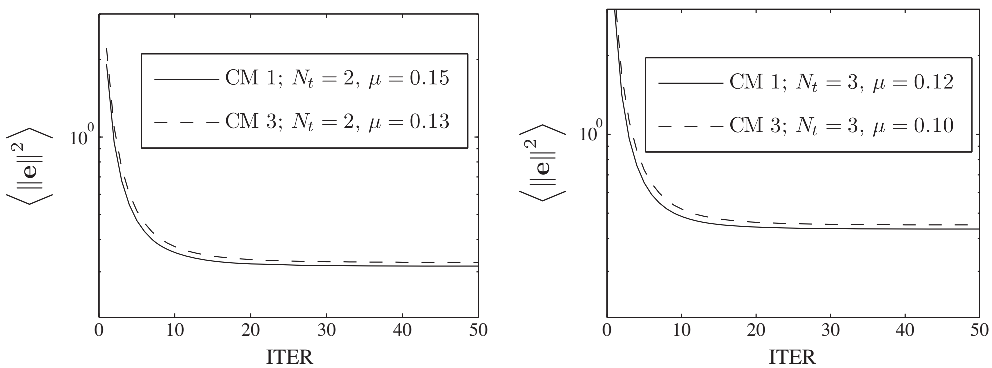

Figure 3. Convergence of the constrained least squares algorithm.

With J_{MMSE} being differentiated with respect to $\bar{\boldsymbol{\gamma}}^*$ and being set to zero,

$$\frac{\partial J_{\text{MMSE}}}{\partial \bar{\boldsymbol{\gamma}}^*} = \frac{1}{SNR}\bar{\boldsymbol{\gamma}} - \mathbf{h}_n + \tilde{\mathbf{H}}^H \tilde{\mathbf{H}} \boldsymbol{\gamma} = 0 \quad (32)$$
$$\Rightarrow \left[\tilde{\mathbf{H}}^H \tilde{\mathbf{H}} + \mathbf{I}\frac{1}{SNR}\right]\bar{\boldsymbol{\gamma}} = \mathbf{h}_n$$

Therefore,

$$\bar{\boldsymbol{\gamma}}_{\text{opt}} = \left[\tilde{\mathbf{H}}^h \tilde{\mathbf{H}} + \mathbf{I}\frac{1}{SNR}\right]^{-1} \mathbf{h}_n \quad (33)$$

where $\mathbf{I}$ is an identity matrix. Finally,

$$\boldsymbol{\gamma} = \boldsymbol{\gamma}^{\text{MMSE}} = \frac{\bar{\boldsymbol{\gamma}}_{\text{opt}}}{\zeta_{\text{opt}}} \Rightarrow \boldsymbol{\gamma}^{\text{MMSE}} = \sqrt{N_t}\,\frac{\bar{\boldsymbol{\gamma}}_{\text{opt}}}{\left\|\bar{\boldsymbol{\gamma}}_{\text{opt}}\right\|_2} \quad (34)$$

The term ζ is just a constant that does not need to be implemented at the receiver side.

Observing Equation (34), one can conclude that if $SNR \to \infty, \bar{\boldsymbol{\gamma}}_{\text{opt}} \to \left(\tilde{\mathbf{H}}^H \tilde{\mathbf{H}}\right)^{-1} \mathbf{h}_n = \left(\tilde{\mathbf{H}}^H \tilde{\mathbf{H}}\right)^{-1} \tilde{\mathbf{H}}^H \mathbf{d}_n$, and, consequently, after normalising the power, $\boldsymbol{\gamma}^{\text{MMSE}} \to \boldsymbol{\gamma}^{ZF'}$. On the other hand, if $SNR \to 0$, $\bar{\boldsymbol{\gamma}}_{\text{opt}} \to C\mathbf{I}\mathbf{h}_n = C\tilde{\mathbf{H}}^H \mathbf{d}_n$, which represents the (L_{PF})th line of $\tilde{\mathbf{H}}$ in Equation (12) multiplied by a constant C, and, therefore, after normalising the power, $\boldsymbol{\gamma}^{\text{MMSE}} \to \boldsymbol{\gamma}^{\boldsymbol{\gamma}^{TR}}$.

3.5. Channel impulse response comparison

Figure 4 shows examples of equivalent CIRs, considering the schemes TR, ZF, MMSE and CLS, with $L_{\text{PF}} = L_{\text{C}}$, but here L_{C} is obtained by considering a truncation criterion of -30 dB (Figure 1); N_{P} is set to $N_{\text{P}} = 100$. The higher *SNR* is obtained with TR (it represents an MF), but the residual ISI is also higher than the other schemes. The ZF pre-equaliser eliminates the ISI but results in a relatively low power at the receiver, which can be interpreted as the dual problem of noise amplification when ZF is used at the receiver side. For the *SNR* conditions considered, the peak of the equivalent CIR with MMSE is a little lower than the case with CLS, but the MMSE scheme results in a somewhat better ISI mitigation.

4. COMPLEXITY ANALYSIS

Table II presents a comparative analysis of the computational complexity for ZF, CLS and MMSE schemes, where $p = (L_{\text{C}} + L_{\text{PF}} - 1)$ and $q = (N_t L_{\text{PF}})$. Complex multiplication (or division), complex addition (or subtraction), square root extraction and comparison are considered as single operations. All multiplications and additions are assumed to be complex operations. For the CLS solution based on SVD, only the operations needed for the computation of SVD are taken into account, which is the most costly part. For a matrix inversion of dimension $N \times N$, the Gaussian elimination method is considered, which requires a total of approximately $2N^3/3$ operations.

5. SIGNAL-TO-INTERFERENCE-PLUS-NOISE RATIO ANALYSIS

Equation (9) can be rewritten as

$$y_n = \sum_{i=-\infty}^{\infty} b_{n-i}x_i + z_n = \underbrace{b_n x_0}_{\text{Signal}} + \underbrace{\sum_{\substack{i=-\infty \\ i\neq 0}}^{\infty} b_{n-i}x_i}_{\text{ISI}} + \underbrace{z_n}_{\text{Noise}} \quad (35)$$

where $y_n = y(nT_s)$, $z_n = z(nT_s)$ and $x_i = x(iT_s)$. Note that the discrete-time sequence that represents the sampled noise after MF, z_n, is still AWGN and with variance (or power) $\sigma_z^2 = N_t\,\sigma_k^2 = N_t/SNR$. The decision variable is $\mathcal{V} = \Re\{y_n\}$, where $\Re\{\cdot\}$ represents the real-part operator. If the information symbols are independent and identically distributed with $b_n = \pm 1$, the instantaneous *SINR* conditioned on the jth set of channel realisations can be obtained as [9]

$$SINR^j = \frac{\Re\{x_0^j\}^2}{\sum\limits_{\substack{i=-\infty \\ i\neq 0}}^{\infty} \Re\left\{x_i^j\right\}^2 + \sigma^2} \quad (36)$$

where $\sigma^2 = \sigma_z^2/2 = N_t/2\,SNR$ represents the variance of the in-phase and quadrature components of z_n.

If the residual ISI in Equation (36) is assumed to be Gaussian distributed, the BER conditioned to the jth set of channel realisations can be written as

$$BER^j = Q\left(\sqrt{SINR^j}\right) \quad (37)$$

where $Q(x) = 1/\sqrt{2\pi} \cdot \int_x^\infty e^{-y^2/2}\,\mathrm{d}y$. Considering $\mathcal{J}$ sets of channel realisations, the average BER can be computed as

$$BER = \frac{1}{\mathcal{J}} \sum_{j=0}^{\mathcal{J}-1} BER^j \quad (38)$$

6. SIMULATION CONFIGURATION AND RESULTS

Performance results are obtained by considering Monte Carlo simulation and the semi-analytical approach (THEO) shown in Section 5. Two and three antenna elements are adopted. The transmission rate is set to $R_b = 499$ Mbps ($\kappa = 4$) and $R_b = 665.3$ Mbps ($\kappa = 3$), and the RRC pulse is generated by considering $\alpha = 0.3$ and $T = 501$ ps. Pre-filter coefficients, as well as the CIR, are assumed to be static during the frame duration T_{f}, which is considered sufficiently long. The CIRs are randomly chosen among the 100 realisations proposed in [16]. $N_{\text{P}} = 100$ probe

Trans. Emerging Tel. Tech. **23**:240–253 (2012) © 2011 John Wiley & Sons, Ltd.
DOI: 10.1002/ett

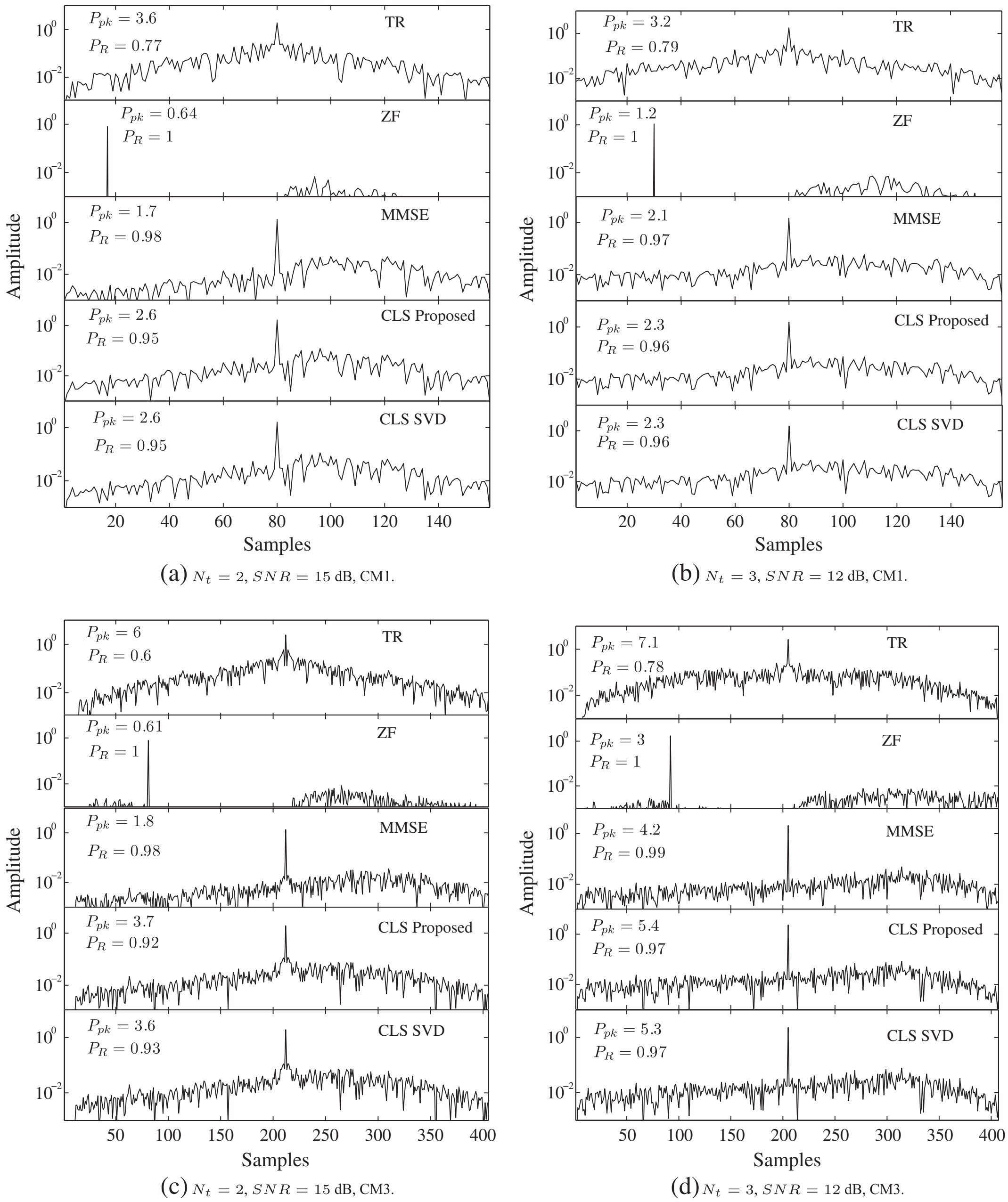

(a) $N_t = 2$, $SNR = 15$ dB, CM1.

(b) $N_t = 3$, $SNR = 12$ dB, CM1.

(c) $N_t = 2$, $SNR = 15$ dB, CM3.

(d) $N_t = 3$, $SNR = 12$ dB, CM3.

Figure 4. Comparison among equivalent channel impulse responses considering time reversal (TR), zero forcing (ZF), minimum mean square error (MMSE) and constrained least squares (CLS), for CM1 and CM3 and $N_P = 100$. P_{pk} represents the peak of the equivalent channel impulse response, whereas P_R is the ratio between P_{pk} and the total power. SVD, singular-value decomposition; SNR, signal-to-noise ratio.

Table II. Computational complexity analysis.

Scheme	Operations needed
ZF	$2p^3/3 + (2q-1)p^2 + (2p-1)(pq+q) + 2q + 1$
MMSE	$2q^3/3 + (2p-1)(q^2+q) + (2q-1)(1+q) + 3q + 3$
CLS (SVD)	$9 \cdot q^3 + 4 \cdot p^2 q + 8 \cdot pq^2$
CLS (Algorithm 3.3)	$\mathrm{ITER} \cdot (4 \cdot pq + 4 \cdot q - p + 2)$

Note that $p = L_C + L_{PF} - 1$ and $q = N_t L_{PF}$.

ZF, zero forcing; MMSE, minimum mean square error; CLS, constrained least squares; SVD, singular-value decomposition.

DOI: 10.1002/ett

transmissions are considered for testing the channel in order to obtain the CIR estimations at the transmitter.

Figures 5 and 6 show the TR, CLS and MMSE analytical BER performances regarding the number of pre-filter coefficients. The CLS scheme is implemented with the modified steepest-descent algorithm considering $ITER = 15$. For $N_t = 2$, $SNR = 15$ dB is set, whereas for $N_t = 3$, $SNR = 12$ dB is set. It is possible to see that in all curves the performances become flat for $L_{\mathrm{PF}} \approx 0.7\, L_{\mathrm{C}}$ with $N_t = 3$ and $L_{\mathrm{PF}} \approx 0.8\, L_{\mathrm{C}}$ with $N_t = 2$.

Bit error rate results as a function of *SNR* in decibels are presented in Figures 7 and 8 for rates $R_b = 665.3$ Mbps

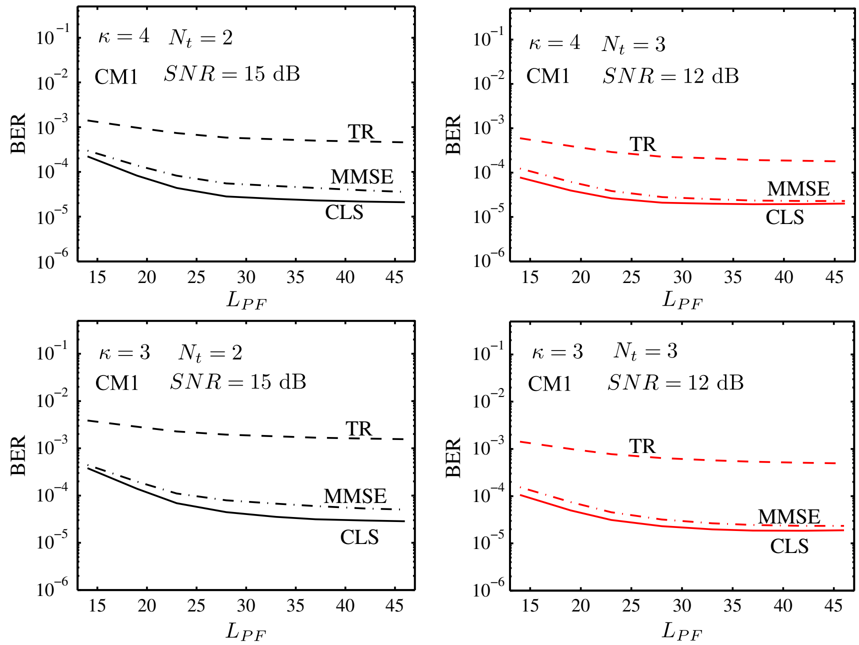

Figure 5. Bit error rate (BER) as a function of L_{PF} considering CM1. TR, time reversal; MMSE, minimum mean square error; CLS, constrained least squares; SNR, signal-to-noise ratio.

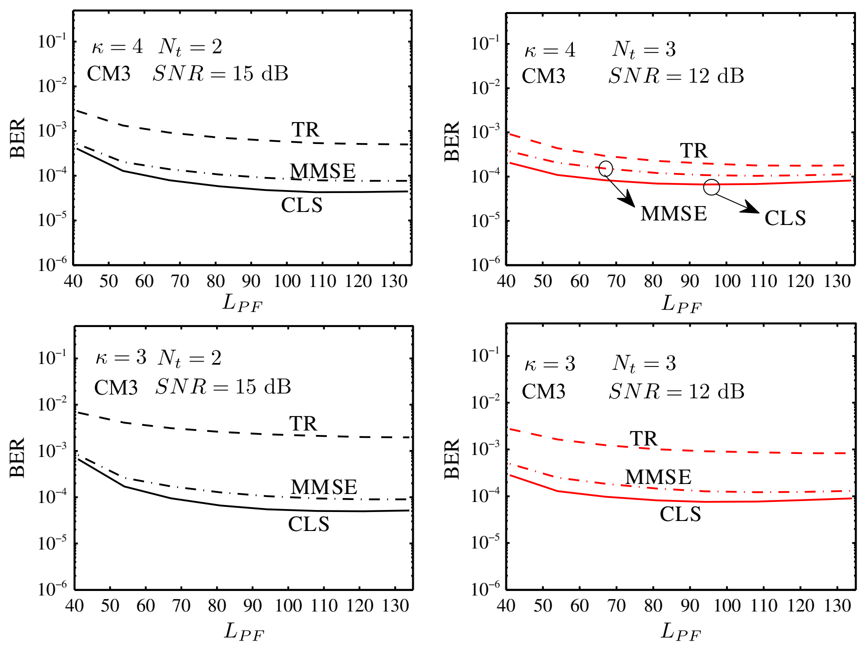

Figure 6. Bit error rate (BER) as a function of L_{PF} considering CM3. TR, time reversal; MMSE, minimum mean square error; CLS, constrained least squares; SNR, signal-to-noise ratio.

Trans. Emerging Tel. Tech. **23**:240–253 (2012) © 2011 John Wiley & Sons, Ltd.
DOI: 10.1002/ett

and $R_b = 499$ Mbps, respectively. In both figures, it was considered that $L_{\mathrm{PF}} \approx 0.7\,L_{\mathrm{C}}$ with $N_t = 3$ and $L_{\mathrm{PF}} \approx 0.8\,L_{\mathrm{C}}$ with $N_t = 2$ for TR, CLS and MMSE, whereas for ZF, $L_{\mathrm{PF}} = L_{\mathrm{C}}$ (ZF$'$ is not considered). Considering the criterion of -20 dB for the CIR truncation, $L_{\mathrm{C}} = 46$ in CM1 and $L_{\mathrm{C}} = 134$ ($+0$ to 5) in CM3. Note that the CLS performance with $ITER = 15$ is superior to the other techniques for $SNR > 9$ dB. For the low-SNR region, TR and MMSE perform better than CLS. The ZF scheme, even for $L_{\mathrm{PF}} = L_{\mathrm{C}}$, has not a satisfactory performance with $N_t = 2$ antennas, but with $N_t = 3$, it is better than TR for high SNRs. Moreover, ZF, MMSE and CLS are less sensitive than TR regarding an increase in the transmission rate from 499 to 665 Mbps.

Table III shows a numerical analysis of the computational complexity considering the configurations presented in Figures 7 and 8. For the ZF scheme, $L_{\mathrm{PF}} = L_{\mathrm{C}}$, and for the CLS with SVD, only the SVD complexity was taken into account. Observe that the method CLS (SVD) is more complex than the other techniques, and ZF has a complexity of the same order as that of MMSE. It is also worth noticing that the CLS method based on the modified steepest-descent algorithm results in a complexity substantially lower than that of the other schemes.

Considering a higher CIR estimation error condition, Figure 9 shows the BER performance for $R_b = 499$ Mbps, $N_t = 2$ antennas and $N_{\mathrm{P}} = 20$. It can be seen that CLS keeps performing better than MMSE. It is possible to see the superiority of CLS in relation to MMSE, as observed in the previous lower CIR estimation error case ($N_{\mathrm{P}} = 100$), specially for higher SNRs.

In order to help us understand why CLS performs better than MMSE under the conditions considered, Figure 10 presents BER versus SNR results considering CM1, $L_{\mathrm{PF}} =$

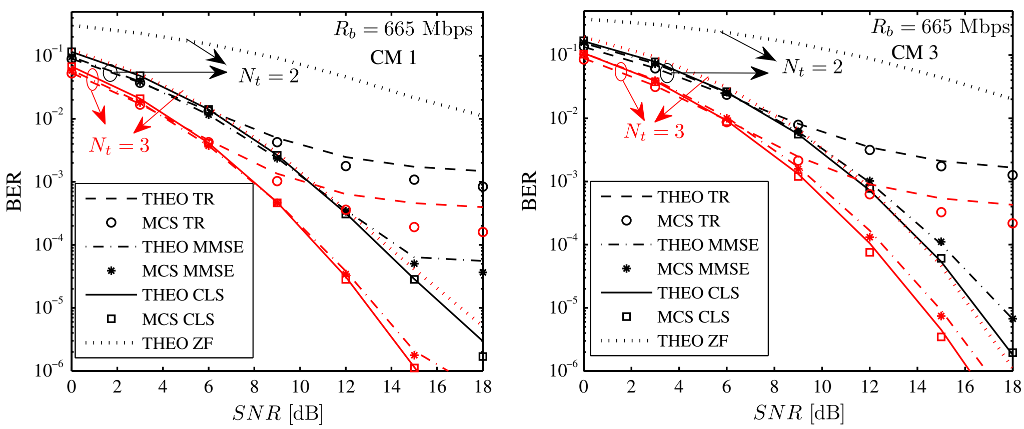

Figure 7. Performance of bit error rate (BER) versus signal-to-noise ratio (SNR) for $R_b = 665.3$ Mbps and $N_{\mathrm{P}} = 100$ probe pulses for channel impulse response estimation. MCS, Monte Carlo simulation; TR, time reversal; MMSE, minimum mean square error; CLS, constrained least squares; ZF, zero forcing.

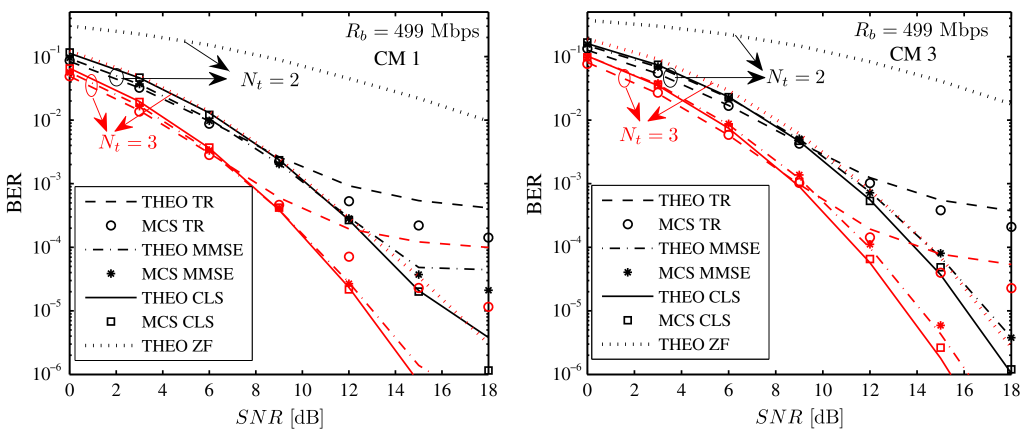

Figure 8. Performance of bit error rate (BER) versus signal-to-noise ratio (SNR) for $R_b = 499$ Mbps and $N_{\mathrm{P}} = 100$ probe pulses for channel impulse response estimation. MCS, Monte Carlo simulation; TR, time reversal; MMSE, minimum mean square error; CLS, constrained least squares; ZF, zero forcing.

Table III. Numerical computational complexity analysis.

Configuration	Number of operations			
	Scheme			
	ZF	MMSE	CLS (SVD)	CLS (mod. grad.)
CM1, $N_t = 2$	2.3342×10^6	1.1697×10^6	9.1030×10^6	3.6565×10^5
CM1, $N_t = 3$	2.6112×10^6	2.0663×10^6	1.6179×10^7	4.5326×10^5
CM3, $N_t = 2$	6.1390×10^7	3.0111×10^7	2.3682×10^8	3.1961×10^6
CM3, $N_t = 3$	6.8684×10^7	5.3298×10^7	4.2041×10^8	3.9619×10^6

ZF, zero forcing; MMSE, minimum mean square error; CLS, constrained least squares; SVD, singular-value decomposition.

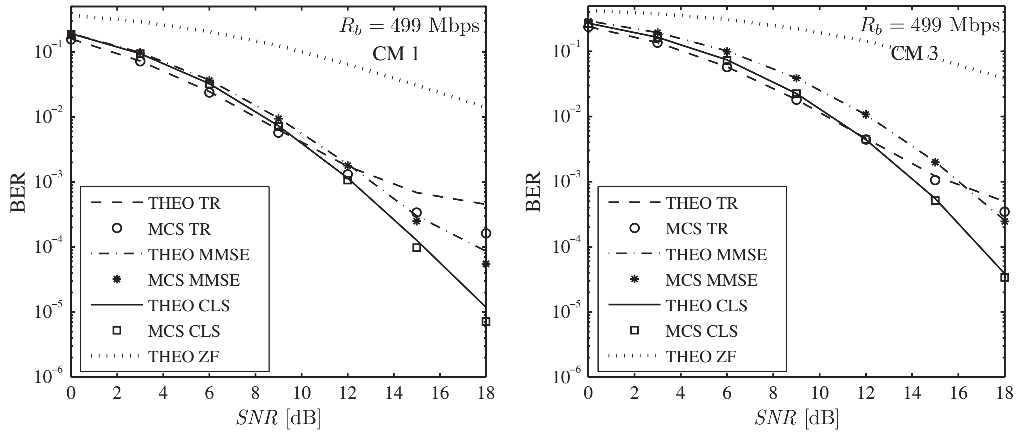

Figure 9. Performance of bit error rate (BER) versus signal-to-noise ratio (SNR) for $R_b = 499$ Mbps, $N_t = 2$ antennas and $N_P = 20$ probe pulses for channel impulse response estimation. MCS, Monte Carlo simulation; TR, time reversal; MMSE, minimum mean square error; CLS, constrained least squares; ZF, zero forcing.

L_C, noiseless CIR estimation at the transmitter and a CIR truncation criterion of −30 dB (Figure 1), which corresponds to 40 ns, approximately, rather than 23 ns (−20-dB criterion). Under these conditions, the performance of MMSE is similar to CLS for $12 < SNR < 16$ dB and slightly better than CLS for $0 < SNR < 12$ dB. Therefore, it is possible to conclude that the CLS scheme is more robust than the MMSE one regarding errors on the CIR estimation (noise and truncation). This observation suggests that the robustness of CLS and MMSE in relation to

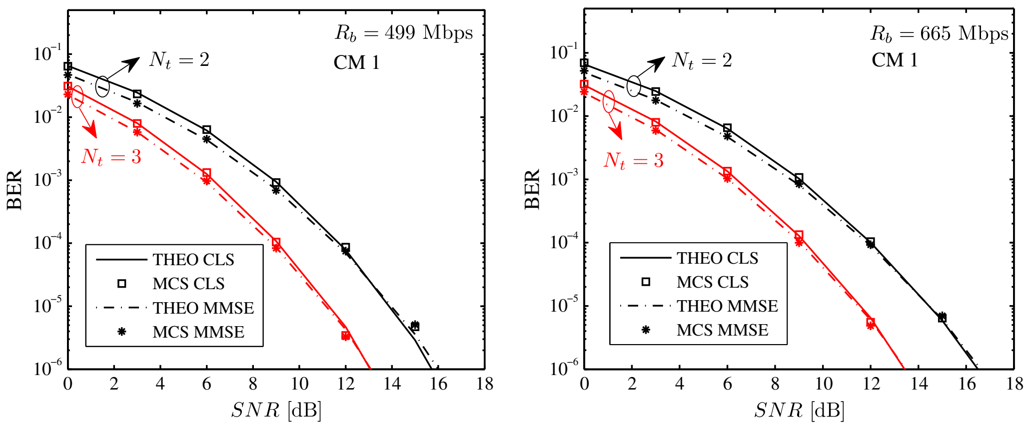

Figure 10. Bit error rate (BER) as a function of signal-to-noise ratio (SNR) in CM1, with noiseless estimation and truncation of the channel impulse response in 40 ns. MCS, Monte Carlo simulation; MMSE, minimum mean square error; CLS, constrained least squares.

Trans. Emerging Tel. Tech. **23**:240–253 (2012) © 2011 John Wiley & Sons, Ltd.
DOI: 10.1002/ett

CIR estimation errors depends on how the respective prefilter coefficients $\boldsymbol{\gamma}_{\mathrm{CLS}}$ and $\boldsymbol{\gamma}_{\mathrm{MMSE}}$ deviate from their ideal noiseless values $\boldsymbol{\gamma}'_{\mathrm{CLS}}$ and $\boldsymbol{\gamma}'_{\mathrm{MMSE}}$, respectively, obtained considering perfect knowledge of the CIR at the transmitter side. In their turn, these deviations can be measured in each case by $\sigma_E^2 = \mathbb{E}\left[\left\|\boldsymbol{\gamma} - \boldsymbol{\gamma}'\right\|^2\right]/L_{\mathrm{PF}}$.

In order to test this dependency, we estimated σ_E^2 for CLS and MMSE, considering different values of SNR (E_b/N_0) and the number of probe transmissions N_{P}. A thousand noisy CIR generations were considered for each simulated point. The results are presented in Figures 11 and 12. It can be seen that CLS performs better than MMSE for higher E_b/N_0 and/or higher N_{P}. Moreover, for higher E_b/N_0 and lower values of N_{P}, CLS is quite better than MMSE. These results are consistent with the BER performance in Figures 7 to 9 and therefore corroborate the dependency of the BER on σ_E^2.

7. CONCLUSIONS

This paper presented a performance analysis for a single-user MISO UWB system incorporating four different predistortion schemes: TR, ZF, MMSE and CLS. Results showed that CLS has a BER performance comparable to that of the MMSE and better than that of TR and ZF. For instance, when $N_t = 2$ antennas, the performance of ZF is not satisfactory because of its power inefficiency, and its performance for $N_t = 3$ antennas is better than that of TR, considering high *SNR*s. Furthermore, when TR is considered for high transmission rates, there is a residual ISI degrading the system's performance, which suggests some post-equalisation scheme at the receiver side.

Under the conditions considered in this paper, it is possible to conclude that the CLS scheme is more robust than the MMSE one regarding errors on the CIR estimation. Besides, the CLS method using the modified gradi-

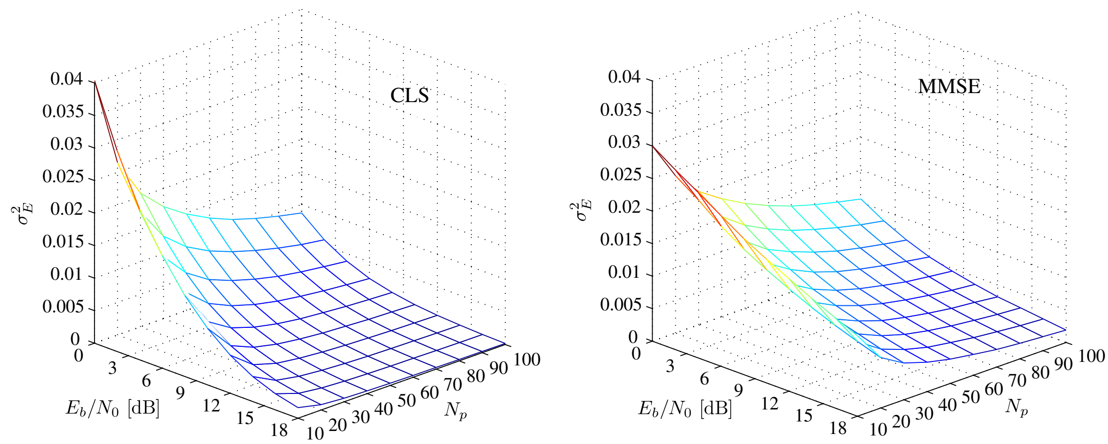

Figure 11. Constrained least squares (CLS) and minimum mean square error (MMSE) sensitivity to channel impulse response errors in CM1, $N_t = 2$ and $R_b = 499$ Mbps.

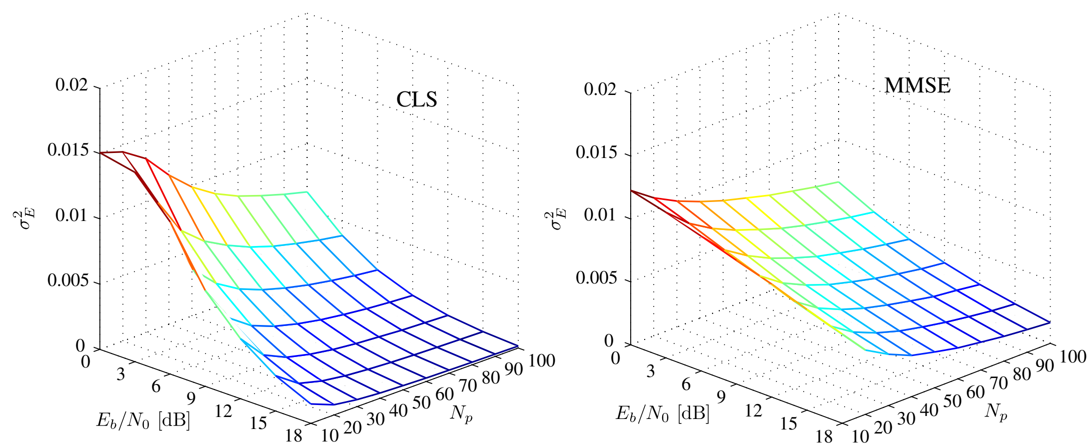

Figure 12. Constrained least squares (CLS) and minimum mean square error (MMSE) sensitivity to channel impulse response errors in CM3, $N_t = 2$ and $R_b = 499$ Mbps.

ent algorithm has a lower complexity compared with ZF and MMSE. Such a scheme could be a good solution for the downlink of high-data-rate applications having good computational capacities at the access point and requiring low-complexity receivers, in no fast varying channels.

ACKNOWLEDGEMENTS

This work was partially funded by the Brazilian agency The National Council for Scientific Technological Development (CNPq, research grant process #303426/2009-8). The authors would like to express gratitude to the Associate Editor and anonymous reviewers for their invaluably constructive suggestions and helpful comments, which have enhanced the readability and quality of the manuscript.

REFERENCES

1. Qiu RC, Zhou C, Guo N, Zhang JQ. Time reversal with MISO for ultrawideband communications: experimental results. *IEEE Antennas and Wireless Propagation Letters* 2006; **5**(1): 269–273.
2. Nguyen HT, Kovács IZ, Eggers PCF. A time reversal transmission approach for multiuser UWB communications. *IEEE Transactions on Antennas and Propagation* 2006; **54**(11): 3216–3224.
3. Guo N, Sadler BM, Qiu RC. Reduced-complexity UWB time-reversal techniques and experimental results. *IEEE Transactions on Wireless Communications* 2007; **6**(12): 4221–4226.
4. Cao W, Nallanathan A, Chai CC. Performance analysis of pre-rake DS UWB multiple access system under imperfect channel estimation. *IEEE Transactions on Wireless Communications* 2007; **6**(11): 3892–3896.
5. Zhou C, Guo N, Sadler BM, Qiu RC. Performance study on time reversed impulse MIMO for UWB communications based on measured spatial UWB channels. In *IEEE Military Communications Conference (MILCOM 2007)*, 2007; 1–6.
6. Kaiser T, Zheng F. *Ultra Wideband Systems with MIMO*. John Wiley and Sons: Chichester, UK, 2010.
7. Strohmer T, Emami M, Hansen J, Papanicolaou G, Paulraj AJ. Application of time-reversal with MMSE equalizer to UWB communications, In *IEEE Global Telecommunications Conference (GLOBECOM '04)*, Vol. 5, 2004; 3123–3127.
8. Song HC, Hodgkiss WS, Kuperman WA, Stevenson M, Akal T. Improvement of time-reversal communications using adaptive channel equalizers. *IEEE Journal of Oceanic Engineering* 2006; **31**(2): 487–496.
9. Angélico BA, Burt PMS, Jeszensky PJE, Hodgkiss WS, Abrão T. Improvement of MISO single-user time reversal ultra-wideband using a DFE channel equalizer, In *10th IEEE International Symposium on Spread Spectrum Techniques and Applications (ISSSTA'08)*, 2008; 582–586.
10. Kyritsi P, Stoica P, Papanicolaou G, Eggers P, Oprea A. Time reversal and zero-forcing equalization for fixed wireless access channels. In *Thirty-Ninth Asilomar Conference on Signals, Systems and Computers*, 2005; 1297–1301.
11. Kyritsi P, Papanicolaou G, Tsogka C. Optimally Designed Time Reversal and Zero Forcing Schemes, In *Proc. Int. Symp. Wireless Personal Multimedia Communication 2005 (WPMC2005)*, September 18-22, 2005; 105–109.
12. Torabi E, Mietzner J, Schober R. Pre-equalization for MISO DS-UWB systems with pre-rake combining. *IEEE Transactions on Wireless Communications* 2009; **8**(3): 1295–1307.
13. Zhiwei L, Xiaoming P, Png KB, Chin F. Kronecker modeling for correlated shadowing in UWB MIMO channels. In *IEEE Wireless Communications and Networking Conference (WCNC 2007)*, 2007; 1583–1587.
14. Fisher R, Kohno R, McLaughlin M, Welbourn M. DS-UWB physical layer submission to IEEE 802.15 Task Group 3a, Jan. 2005. Doc. number P802.15-04/0137r4, April IEEE P802.15.
15. IEEE. IEEE 802.15.4a-2007. Part 15.4: wireless Medium Access Control (MAC) and physical layer (PHY) specifications for low-rate wireless personal area networks (WPANs). Amendment 1: add alternate PHYs, April 2007.
16. Foerster JR. Channel Modeling Sub-committee report final. IEEE P802.15-02/368r5-SG3a, IEEE P802.15 Working Group for Wireless Personal Area Networks (WPAN), Dec. 2002.
17. Molisch AF, Foerster JR, Pendergrass M. Channel models for ultrawideband personal area networks. *IEEE Wireless Communications* 2003; **10**(6): 14–21.
18. Golub GH, Van Loan CF. *Matrix Computations*, 3rd edn. Johns Hopkins University Press: Baltimore, MD, USA, 1996.

AUTHORS' BIOGRAPHIES

B. A. Angélico received the BS degree in Electrical Engineering from the State University of Londrina in 2003 and the MS and and PhD degrees in Electrical Engineering from Escola Politécnica of the University of São Paulo (EP-USP) in 2005 and 2010, respectively. He was a visiting scholar at the California Institute for Telecommunications and Information Technology (Calit2), University of California, San Diego in 2007-2008. He is currently an Assistant Professor at the Federal University of Technology-Paraná. His research interests include ultra-wideband, multiple-input, multiple-output systems, spread spectrum and multi-user detection.

Trans. Emerging Tel. Tech. **23**:240–253 (2012) © 2011 John Wiley & Sons, Ltd.
DOI: 10.1002/ett

P. J. E. Jeszensky received the BS, MS and PhD degrees, all in Electrical Engineering from Escola Politécnica of University of São Paulo (EPUSP, Brazil), in 1972, 1981 and 1989, respectively. Since 1990, he has been with EPUSP where he is a Full Professor and a Researcher in Communication Systems. He was a visiting professor at Universitat Politécnica de Catalunya (UPC), Barcelona (Spain) in 1995 and at Technical University of Budapest (TUB, Hungary) in 2001. He is the author of the book Sistemas Telefônicos (in Portuguese), Editora Manole, 2003, and his current research interests include code division multiple access systems, multi-user detection, code sequences analysis and related topics.

P. M. S. Burt received bachelor, master and doctoral degrees in Electrical Engineering from the University of São Paulo (Escola Politécnica), São Paulo, Brazil, where he has been since 1992 and where he is currently an Associate Professor. From 1984 to 1992, he worked in the telecommunications industry as a development engineer. In 2003, he spent a sabbatical year at the Institut National des Télécommunications, Evry, France. His research interests include adaptive signal processing, telecommunications applications and processing of acoustic signals.

W. S. Hodgkiss received the BSEE degree from Bucknell University, Lewisburg, PA, in 1972, and the MS and PhD degrees in Electrical Engineering from Duke University, Durham, NC, in 1973 and 1975, respectively. From 1975 to 1977, he worked with the Naval Ocean Systems Center, San Diego, CA. From 1977 to 1978, he was a faculty member in the Electrical Engineering Department, Bucknell University. Since 1978, he has been a member of the faculty of the Scripps Institution of Oceanography, University of California, San Diego, and on the staff of the Marine Physical Laboratory. Currently, he is the Deputy Director, Scientific Affairs, Scripps Institution of Oceanography. His present research interests are in the areas of signal processing, propagation modeling and environmental inversions with applications of these to underwater acoustics and electromagnetic wave propagation. Dr Hodgkiss is a Fellow of the Acoustical Society of America.

T. Abrão received the BS, MSc and PhD degrees, all in Electrical Engineering from Escola Politécnica of University São Paulo (EPUSP), Brazil, in 1992, 1996 and 2001, respectively. He is currently an Adjunct Professor at the Electrical Engineering Department of UEL-State University of Londrina (Brazil). Currently (2007/2-2008/1), he is a visiting professor at TSC/UPC-Department of Signal Theory and Communications, Universitat Politécnica de Catalunya, Barcelona, Spain. His research interests include multi-user detection, multi-carrier code division multiple access and multiple-input multiple-output systems, heuristic and optimization aspects of direct-sequence code division multiple access systems and 4G systems. He is author or co-author of more than 80 research papers published in specialized periodicals and symposiums.